Hindawi
International Journal of Photoenergy
Volume 2019, Article ID 5329086, 12 pages
https://doi.org/10.1155/2019/5329086

Research Article

Form and Operation Mode Analysis of a Novel Solar-Driven Cogeneration System with Various Collector Types

Haofei Zhang, Bo Lei, Tao Yu, and Zhida Zhao

School of Mechanical Engineering, Southwest Jiaotong University, Chengdu 610031, China

Correspondence should be addressed to Bo Lei; lbswjtu@163.com

Received 11 November 2018; Accepted 20 February 2019; Published 11 April 2019

Academic Editor: Santolo Meo

In this study, the form and operation modes of a novel solar-driven cogeneration system consisted of various solar collectors (flat plat collectors (FPC), evacuated tube collectors (ETC), and parabolic trough collectors (PTC)) and ORC (organic Rankine cycle) based on building heating load are analyzed. This paper mainly obtains the fitting formula of thermal efficiency of the ORC power generation device and determines the form and operation mode of the cogeneration system. The form is the same, but the operation modes are different for PTC and FPC or ETC. There are six operating modes, respectively, based on the size relationship between the heating load of buildings and the effective heat collection of the solar collector subsystem when the solar collectors are PTC or FPC and ETC.

1. Introduction

Solar energy is a reliable energy, and the solar water heating system is one of the applications of solar energy which has drawn a great attention in this field. But the solar water heating technology has some problems like the system is not utilized in nonheating season and the equipment utilization rate is low. Due to the idle of the solar water heating system and the lack of operation and maintenance, the solar water heating system has a low service life and poor reliability. Wang et al. [1] conducted a follow-up investigation and analysis of 28 solar water heating systems in Tibet, and the results showed that most of them were in a state of paralysis after about 3 years of operation, which was then replaced by the high-energy fuel boiler or electric boiler heating system. One of the most important reasons is that the solar collector system is idle in nonheating season and lacks operation and maintenance.

If the idle solar collector system can be fully utilized and the solar radiation can be converted into available electric energy in nonheating season, it can not only improve the reliability of solar water heating system and increase the utilization rate of the equipment but also reduce the local consumption of petrochemical energy.

However, the outlet temperature of the solar collectors for the heating system is low for thermal power generation based on the Rankine cycle. Organic Rankine cycle (ORC) enables an efficient power generation unit from low-grade heat sources by replacing water with organic working fluids, such as refrigerants or hydrocarbon. Thus, the solar collectors and ORC can form a solar thermal power generation system in nonheating season and a solar-driven cogeneration system in heating season. This paper mainly discusses the solar-driven cogeneration system consisted of the solar collectors and ORC.

Through literature review, there are very few studies on the combination of the solar collector and ORC thermal generator set to realize heating and power generation, and the research mainly lies in the thermodynamic analysis of the system [2–12]. Zhai et al. [2] studied a novel hybrid solar trigeneration system based on the use of a parabolic trough collector (PTC), a screw expander, and a silica gel-water adsorption cooling module in Dunhuang, China. The energy and exergy efficiencies of the system were estimated at 58% and 15.2%, respectively. Al-Sulaiman et al. [3–5] studied a novel trigeneration system using the parabolic trough collectors and an ORC, which used the solar energy to heat the organic working medium to generate steam to drive the

turbine to generate power and at the same time used the waste heat of steam for heating and cooling. Since the solar radiation intensity varies with time throughout the day, the operating mode of the system is divided into three parts, namely, solar mode, storage mode, and solar and storage mode, and the thermoelectric conversion efficiency and cogeneration thermal efficiency of each operation mode are analyzed. The results show that the maximum thermal efficiency of solar mode is 15% and the maximum cogeneration thermal efficiency is 94%. The maximum thermal efficiency of solar and storage mode is 7%, and the maximum cogeneration thermal efficiency is 47%. The maximum thermal efficiency of the storage mode is 6.5%, and the maximum cogeneration thermal efficiency is 42%. Wang [6] analyzed a novel modular system combining cooling, heating, and power generation and found that when the output electricity is constant, the overall efficiencies of energy and exergy of the system operating at the CCHP mode are 9.37 times and 2.62 times as big as those of the system operating at the solar thermal power mode. Al-Ali and Dincer [7] investigated a multigenerational integrated geothermal-solar system with two ORCs and an absorption chiller to produce electrical power, cooling, space heating, and hot water. The energy and exergy efficiencies of the system were found to be 78% and 36.6%, respectively. Kalogirou et al. [8, 9] presented a review of exergy analysis of solar thermal collectors and processes and pointed out that exergy analysis is a valuable method to evaluate and compare possible configurations of solar-driven trigeneration systems. Bellos and Tzivanidis [10] investigated a solar-driven trigeneration system using the parabolic trough collectors, an ORC, and an absorption heat pump operating with the LiBr-H_2O working pair. They studied eight different working fluids and six extra design parameters and found that toluene is the working fluid which leads to maximum exergetic output with n-octane and MDM to follow with 29.42%, 28.50%, and 28.35%, respectively. Freeman et al. [11] examined a domestic-scale solar combined heating and power system with an ORC engine and a nonconcentrated solar thermal collector array. They found that R245ca has the highest net annual work output of the investigated working fluids. Zhang et al. [12] compared two kinds of solar-driven cogeneration systems in Lhasa and found that parallel mode is superior to the series mode when the solar collector is FPC and series mode is superior to the parallel mode when the solar collector is PTC and when the solar collector is ETC; it depends on the temperature of the return heating water.

A few studies have examined the solar collectors integrated with an ORC for electrical power production [13–21]. Delgado-Torres and García-Rodríguez [13] carried out thermodynamic investigations of a solar ORC with four different models of stationary solar collectors by comparing various working fluids. Results showed that the system has the highest overall energetic efficiency for the working fluids R245ca and R245fa. Wang et al. [14, 15] proposed and tested a low-temperature solar ORC system utilizing R245fa as the working fluid. The overall power generation efficiency was 4.2% when the solar collectors were the evacuated tube collectors (ETC), while it was 3.2% under the condition of flat plat collectors (FPC). He et al. [16] built a model for a typical thermal power generation system with the PTC and ORC within the transient energy simulation package TRNSYS and found that pentane had the best performance among three organic working fluids, R113, R123, and pentane. Pei et al. [17, 18] found that the overall electrical efficiency was about 8.6% when a solar irradiation of 750 W/m^2 was assumed in a low-temperature solar thermal electric generation system based on compound parabolic collectors (CPC) and ORC. Cau and Cocco [19] evaluated the annual performance of a 1 MW solar ORC plant comparing parabolic trough with linear Fresnel solar collectors and found that the linear Fresnel collectors lead to higher values of electrical energy production per unit area of occupied land. Ruzzenenti et al. [20] conducted a life cycle and an exergy life cycle analysis for microscale geothermal-solar ORC plants for cogeneration of power and heat. Baccioli et al. [21] studied the dynamic behavior of a small solar plant with static compound parabolic collectors and an ORC in Italy. It was found that the specific production of the plant increases with the concentration ratio and with the decrease of latitude.

According to the literature review, there is no corresponding study on the form and the operating mode of the solar-driven cogeneration system consisted of solar collectors and ORC based on building heating load.

This paper mainly discusses the form and operation mode of the solar-driven cogeneration system with various collector types.

2. System Descriptions

This paper mainly analyzes the following two aspects:

(1) When the building heating load (refers to the daily accumulated heat load of the building) is greater than the effective heat collection (daily heat collection) of the solar collectors, form (a) or form (b) should be adopted, as shown in Figure 1. Form (a) can generate electricity, if the auxiliary heat source for air source heat pump is equivalent to reduce the energy consumption of air source heat pump. Therefore, the total heat provided by the form is equivalent to the heat generated by condensation heat of the ORC subsystem plus the heat of the air source heat pump driven by the generated electricity of the ORC subsystem. While in form (b), the collector can run at a lower temperature, with higher efficiency, so more effective heat collection can be obtained

(2) zWhen the building heating load (refers to the daily accumulated heat load of the building) is less than the effective heat collection (daily heat collection) of the solar collectors, form (a) or form (b) should be adopted, as shown in Figure 2. In form (a), the hot fluid from the solar collection and heat storage subsystem enters the ORC subsystem to generate electricity. The condensing heat is partly used for

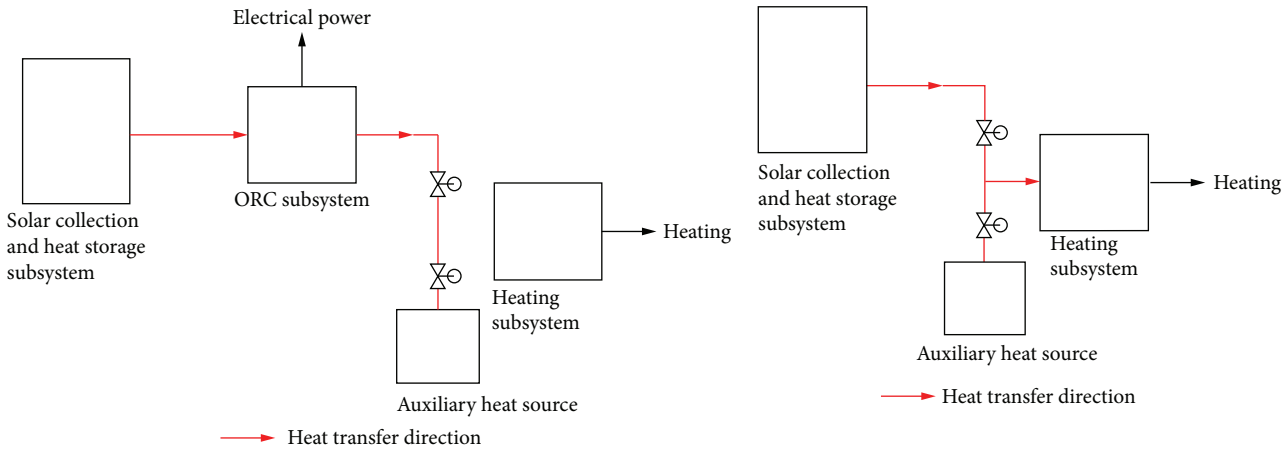

(a) Solar-driven cogeneration system (form (a))

(b) Solar heating system (form (b))

Figure 1: Forms when the building heating load is greater than the effective heat collection.

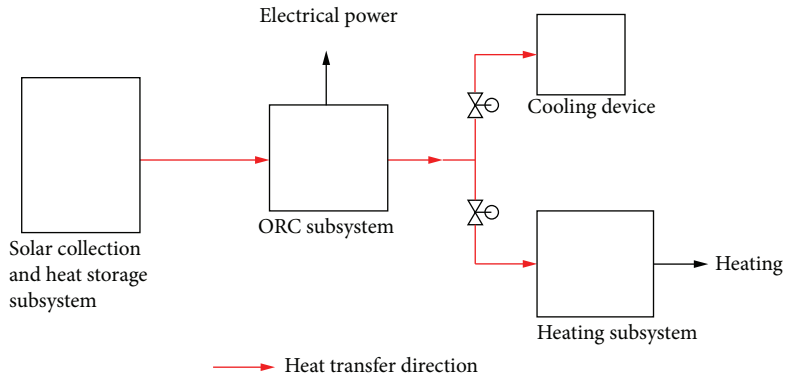

(a) Solar-driven cogeneration system with a cooling device (form (c))

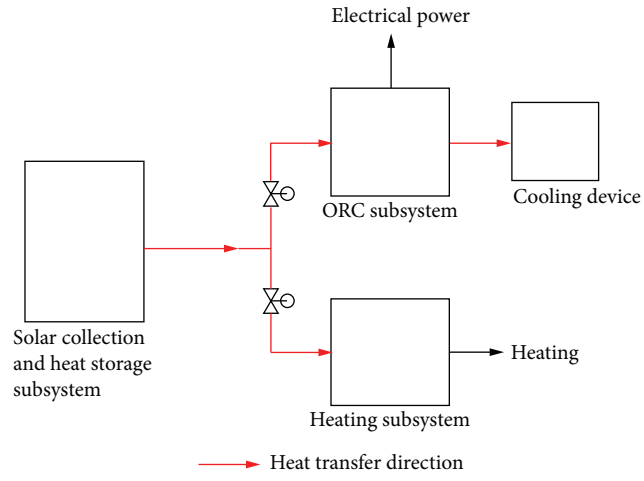

(b) Solar thermal power generation combined with the solar heating system (form (d))

Figure 2: Forms when the building heating load is less than the effective heat collection.

heating and partly cooled by the cooling device. This form makes full use of energy cascade utilization, but the efficiency of the ORC subsystem is low due to the heat supply temperature limitation. In form (b), the hot fluid from the solar collection and heat storage subsystem is partly used for heating and partly for solar power generation. The condensing temperature of the ORC subsystem can be greatly reduced, and the power generation efficiency is higher

For the convenience of analysis, this paper makes the following assumptions:

(1) The solar collector subsystem and the heat storage subsystem are considered as a whole, and the heat loss of the heat storage subsystem is not taken into account, so the heat collection of the solar collector subsystem is stored by the heat storage subsystem when there is surplus

(2) Energy conservation when heat energy is transferred between modules

(3) The energy consumption of the circulating pump of the heat storage subsystem and heat supply subsystem is not considered

(4) It is assumed that the temperature difference between the inlet and the outlet of the solar collector, the temperature difference between the inlet and the outlet of the ORC subsystem, and the temperature difference of the heating circulating water are equal

(5) The auxiliary heat source is air source heat pump

(6) The time unit of analysis is day

3. Mathematical Modeling

3.1. Solar Collection and Heat Storage Subsystem. The effective heat collection of the solar collector subsystem can be calculated as follows:

$$Q_{use} = Q_{sol} \cdot \eta_{col} = A_{col} \cdot G_{eff} \cdot \eta_{col} = c_{p,col} \cdot m_{col} \cdot (t_{col,out} - t_{col,in}), \quad (1)$$

where A_{col} and G_{eff} represent the area of the solar collector subsystem and the effective radiation on them. η_{col} represents the efficiency of solar collectors. $c_{p,col}$ and m_{col} represent the specific heat at constant pressure and the mass flow rate of the fluid in the solar collectors, respectively. $t_{col,in}$ and $t_{col,out}$ represent the inlet and outlet temperature of the solar collectors.

η_{col} is generally calculated by equation (2) and the corresponding coefficients a_0, a_1, and a_2 are given by experiments.

$$\eta_{col} = \frac{a_0 - a_1(t_{col,in} - t_a)}{G_{eff} - a_2(t_{col,in} - t_a)^2 / G_{eff}}, \quad (2)$$

where t_a represents the ambient temperature, ˚C.

Coefficients a_0, a_1, and a_2 are given in the literatures [22–26], and the specific values are shown in Table 1.

As can be seen in Table 1, a_0 is basically between 0.7 and 0.8, with little change, while a_1 varies widely. For FPC and ETC, a_2 is generally not considered. For PTC, when the temperature of solar collectors in 120~150˚C, approximately equation (3) can be derived. Therefore, this paper mainly analyzes the influence of the value of a_1 on the form of the cogeneration system.

$$\frac{a_1(t_{col,in} - t_a)}{G_{eff}} = \frac{a_2(t_{col,in} - t_a)^2}{G_{eff}}. \quad (3)$$

3.2. ORC Subsystem. The thermal process of the ORC subsystem is shown in Figure 3.

The process 5-1 in the evaporator is given by equation (4). The pinch point temperature of the evaporator can be described as equation (5).

$$Q_{evap} = m_{org} \cdot (h_1 - h_5) = c_{p,col} \cdot m_{col} \cdot (t_{R,in} - t_{R,out}), \quad (4)$$

$$\Delta t_{evap} = t_8 - t_6. \quad (5)$$

Process 1–2 in the screw expander is given as follows:

$$W_{SE} = m_{org} \cdot (h_1 - h_2) \cdot \eta_{SE,ise} \cdot \eta_{SE,mec}. \quad (6)$$

Process 2-4 in the condenser is given as follows:

$$Q_{cond} = m_{org} \cdot (h_2 - h_4) = c_{p,wat} \cdot m_{wat} \cdot (t_{L,out} - t_{L,in}). \quad (7)$$

The pinch point temperature of the condenser can be described as follows:

$$\Delta t_{cond} = t_3 - t_9. \quad (8)$$

Process 4–5 in the ORC pump is given as follows:

$$W_{OP} = \frac{m_{org} \cdot (h_5 - h_4)}{\eta_{OP,ise} \cdot \eta_{OP,mec}}. \quad (9)$$

The net power output of the ORC system is as follows:

$$W_{ORC} = W_{SE} - W_{OP}. \quad (10)$$

The thermal efficiency of the ORC system can be calculated as follows:

$$\eta_{ORC} = \frac{W_{ORC}}{Q_{evap}} = \frac{W_{SE} - W_{OP}}{c_{p,col} \cdot m_{col} \cdot (t_{R,in} - t_{R,out})}. \quad (11)$$

3.3. Cooling Device. According to the literature [27], the power consumption of the cooling device is given by equation (12), where w_{cond} is the power consumption of the cooling device per unit cooling load.

$$W_{cond} = Q_{cond} \cdot w_{cond}. \quad (12)$$

3.4. Auxiliary Heat Source. The auxiliary heat source adopts CO_2 air source heat pump; COP of which is mainly related to the ambient temperature (t_a) and the outlet temperature (t_c) of hot water. According to the product sample provided by the equipment manufacturer, the surface model of the COP of the CO_2 air source heat pump is obtained, as shown in Figure 4. The calculation formula of COP is given as follows:

$$COP = 0.026 \cdot t_a - 0.011 \cdot t_c + 3.256. \quad (13)$$

Table 1: Coefficients a_0, a_1, and a_2.

Collector type	a_0	a_1	a_2	Test conditions (flow rate per unit area (kg/s m^2), collector slope angle)	Reference
FPC	0.79	6.67	/	0.015, 40°	[22]
	0.80	4.78	/	0.015, 40°	[23]
	0.7156	4.149	/	0.02, 30°	[24]
	0.7455	5.8512	/	/	[25]
ETC	0.82	2.19	/	0.014, 40°	[22]
	0.7541	2.2258	/	/	[25]
	0.722	2.20	/	0.011, 40°	[26]
	0.742	2.76	/	0.011, 40°	[26]
PTC	0.762	0.2125	0.001672	0.015, single axis tracking	[22]

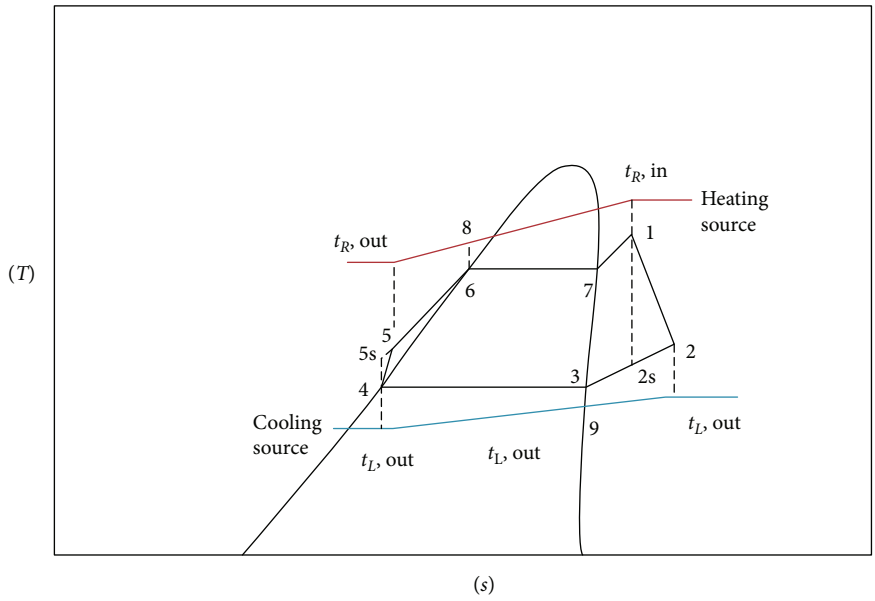

Figure 3: T-s diagram of ORC.

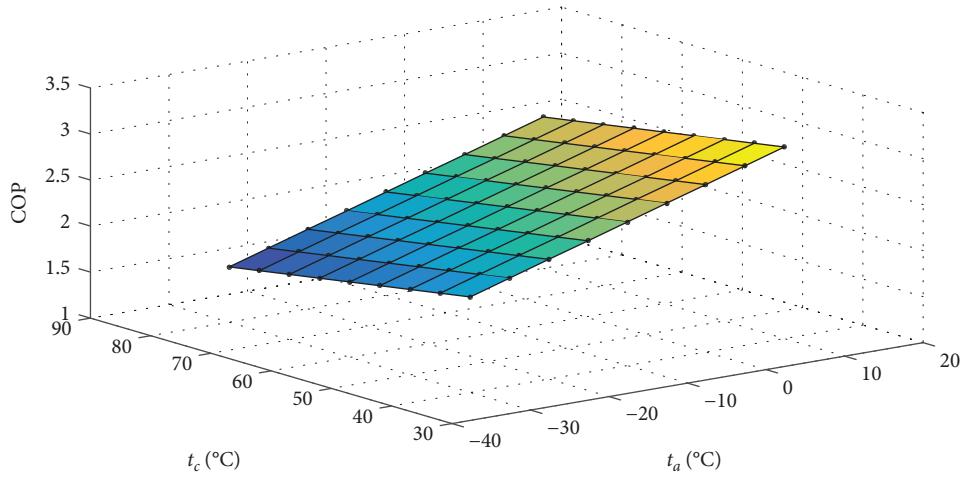

Figure 4: COP of the CO_2 air source heat pump.

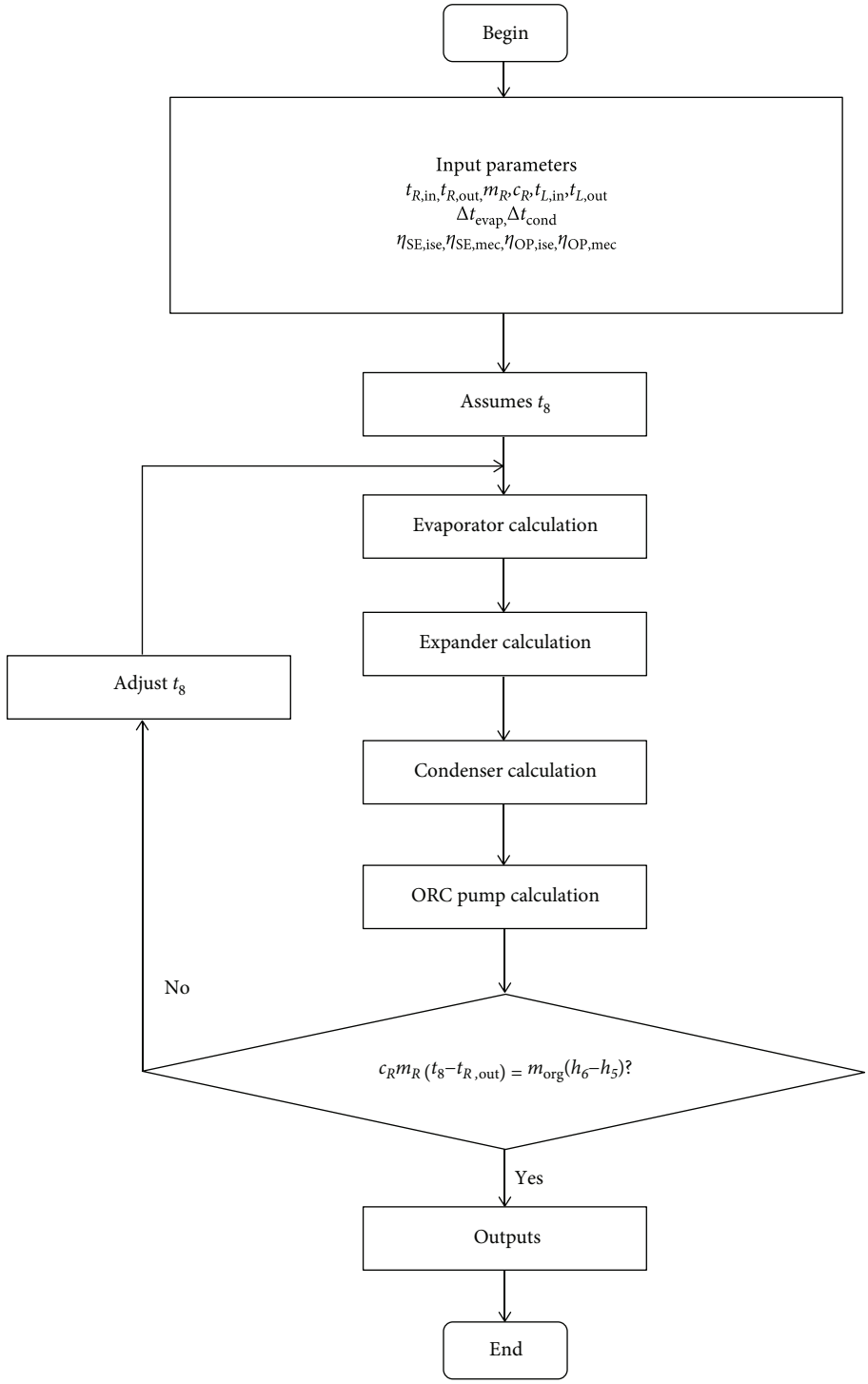

Figure 5: The calculation flow chart of the ORC subsystem.

3.5. Heating Subsystem. The formula described the heating subsystem as follows:

$$Q_{\text{load}} = c_{\text{wat}} \cdot m_{\text{wat}} \cdot \left(t_{n,g} - t_{n,h}\right), \tag{14}$$

where Q_{load} represents heating load of buildings. c_{wat} and m_{wat} represent the specific heat and the mass flow rate of heating water. $t_{n,g}$ and $t_{n,h}$ represent the supply and return water temperature of heating water.

4. Analysis and Discussion

4.1. Reduced Model of the ORC Subsystem. According to the mathematical model shown in Section 3.2, a calculation program with MATLAB and REFPROP is developed in this

paper. The calculation flow chart is shown in Figure 5. Some input parameters are shown in Table 2.

In order to verify the accuracy of the calculation model, the calculation results and the experimental data provided by the equipment manufacturer are compared at the same condition, as shown in Table 3. And the experimental site is shown in Figure 6.

From Table 3, it can be seen that the relative error is less than 5%, indicating that the calculated model is reliable.

According to the program, after some calculation, this paper obtained the surface model of the thermal efficiency of the ORC subsystem when the temperature difference is 5°C between the inlet and outlet of the evaporator, as shown in Figure 7. The calculation formula of thermal efficiency is given as follows:

$$\eta_{\mathrm{ORC}} = -9.876641 \times 10^{-8} \cdot {t_{R,\mathrm{out}}}^3 + 2.663507 \times 10^{-5} \cdot {t_{R,\mathrm{out}}}^2 - 0.001426 \cdot t_{R,\mathrm{out}} + 5.161472 \times 10^{-6} \cdot {t_{L,\mathrm{in}}}^2 - 0.001676 \cdot t_{L,\mathrm{in}} + 0.091751. \quad (15)$$

When the temperature difference is not 5°C between the inlet and outlet of the evaporator, the thermal efficiency of the ORC subsystem has a linear relationship with the temperature difference of thermal fluid inlet and outlet of the evaporator, as shown in Figure 8.

Finally, the calculation formula of thermal efficiency is given as follows:

$$\eta_{\mathrm{ORC}} = -9.876641 \times 10^{-8} \cdot {t_{R,\mathrm{out}}}^3 + 2.663507 \times 10^{-5} \cdot {t_{R,\mathrm{out}}}^2 - 0.001726 \cdot t_{R,\mathrm{out}} + 5.161472 \times 10^{-6} \cdot {t_{L,\mathrm{in}}}^2 - 0.001676 \cdot t_{L,\mathrm{in}} + 0.0003 \cdot t_{R,\mathrm{in}} + 0.090251. \quad (16)$$

4.2. Form and Operation Mode Analysis of the Cogeneration System

4.2.1. When the Building Heating Load Is Greater than the Effective Heat Collection. The total heat supply of form (a) can be calculated as follows:

$$Q_{\mathrm{fa}} = Q_{\text{use-fa}} \cdot (1 - \eta_{\text{ORC-}n}) + Q_{\text{use-fa}} \cdot \eta_{\text{ORC-}n} \cdot \mathrm{COP}, \quad (17)$$

where $Q_{\text{use–fa}}$ represents the effective heat collection of the solar collector subsystem and the inlet temperature when the power generation is maximum. $\eta_{\text{ORC–}n}$ represents the thermal efficiency of the ORC subsystem when $t_{L,\mathrm{in}}$ is $t_{n,h}$.

The total heat supply of form (b) can be calculated as follows:

$$Q_{\mathrm{fb}} = Q_{\text{use-}n}, \quad (18)$$

Table 2: Input values of parameters.

Parameters	Input value	Parameters	Input value
Organic fluid	R245fa	$\eta_{\mathrm{SE,mec}}$ (%)	0.90
Δt_{evap} (°C)	3	$\eta_{\mathrm{OP,ise}}$ (%)	0.70
Δt_{cond} (°C)	3	$\eta_{\mathrm{OP,mec}}$ (%)	0.70
$\eta_{\mathrm{SE,ise}}$ (%)	0.85	w_{cond}	11.12 W/kW

Table 3: Comparison of the calculation model and the experiment.

Parameters	Experiment	Calculation model	Relative error
$t_{R,\mathrm{in}}$ (°C)	95.03	95.03	/
Flow rate of heat source (t/h)	77.94	77.94	/
$t_{R,\mathrm{out}}$ (°C)	74.08	74.08	/
t_a (°C)	25	25	/
$t_{L,\mathrm{in}}$ (°C)	23.39	23.39	/
$t_{L,\mathrm{out}}$ (°C)	30.41	30.41	/
t_{evap} (°C)	76.62	77.08	0.60%
t_{cond} (°C)	32.41	32	−1.27%
Q_{evap} (kW)	1905	1905	/
Q_{cond} (kW)	1736	1703	−1.90%
W_{SE} (kW)	151.35	154.94	2.37%
W_{OP} (kW)	8.83	8.57	−2.94%
W_{ORC} (kW)	141.86	146.37	3.18%
η_{ORC} (%)	7.45	7.68	3.09%

Figure 6: The experimental site of the ORC thermal power plant of the manufacturer.

where $Q_{\text{use–}n}$ represents the effective heat collection of the solar collector subsystem and the inlet temperature is $t_{n,h}$.

$$\Delta Q = Q_{\mathrm{fa}} - Q_{\mathrm{fb}}. \quad (19)$$

If the value of ΔQ is greater than 0, then form (a) is better than form (b); on the other hand, form (b) is better.

After the calculation, it can be obtained as follows:

$$\Delta Q = f(a_0, a_1, G_{\mathrm{eff}}, t_a, t_{n,h}). \quad (20)$$

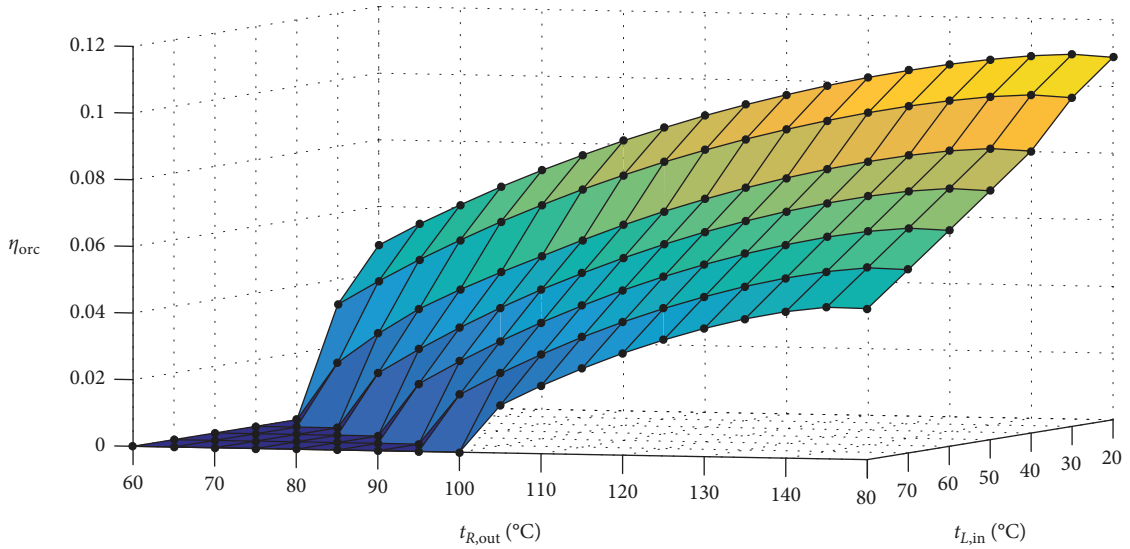

Figure 7: Thermal efficiency of the ORC subsystem ($t_{R,in}$-$t_{R,out}$ = 5°C).

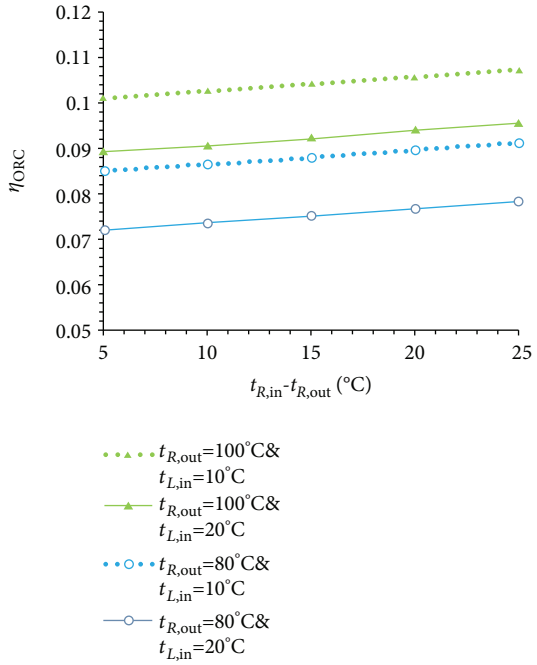

Figure 8: Thermal efficiency of the ORC subsystem along with the temperature difference of thermal fluid inlet and outlet of the evaporator.

For the Lhasa region, the average effective solar radiation G_{eff} and the average ambient temperature t_a are determined values and the value range of a_0 does not change much. Therefore, this paper mainly analyzes the influence of the value of a_1 and the value of $t_{n,h}$ on the form of the cogeneration system.

Figure 9 shows the value of ΔQ and the inlet temperature of form (a) under different a_1 and $t_{n,h}$. It can be seen that with the increase of a_1, the value of ΔQ decreases quickly at first and then slowly increases at some point and the inlet temperature of form (a) gradually reduces. Therefore, when a_1 is greater than 4.0, the thermal efficiency of the ORC subsystem is very low, which means that the form (a) cannot be adopted.

The value of ΔQ is greater than 0 when a_1 is less than 0.45, and only PTC meets the condition from Table 1. That is, form (a) is better for PTC and form (b) is better for FPC and ETC.

4.2.2. When the Building Heating Load Is Less than the Effective Heat Collection. The total power generation of form (c) can be calculated as follows:

$$W_{fc} = Q_{use} \cdot \eta_{ORC\text{-}n} - [Q_{use}(1 - \eta_{ORC\text{-}n}) - Q_{load}] \cdot w_{cond}. \quad (21)$$

The total power generation of form (d) can be calculated as follows:

$$W_{fd} = (Q_{use} - Q_{load}) \cdot \eta_{ORC\text{-}a} - (Q_{use} - Q_{load})(1 - \eta_{ORC\text{-}a}) \cdot w_{cond}, \quad (22)$$

where η_{ORC-a} represents the thermal efficiency of the ORC subsystem when $t_{L,in}$ is the value of return water temperature of the cooling device.

$$\Delta W = W_{fc} - W_{fd}. \quad (23)$$

If the value of ΔW is greater than 0, then form (c) is better than form (d); on the other hand, form (d) is better.

After the calculation, it can be obtained as follows:

$$\Delta W = Q_{use}(1 + w_{cond}) \left[\eta_{ORC\text{-}n} - \left(1 - \frac{Q_{load}}{Q_{use}}\right)\eta_{ORC\text{-}a}\right]. \quad (24)$$

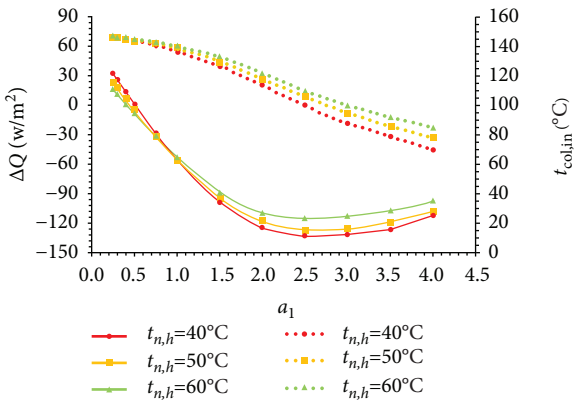

Figure 9: The value of ΔQ and the inlet temperature of form (a) under different a_1 and $t_{n,h}$.

It is thus possible to obtain

$$\frac{Q_{\text{load}}}{Q_{\text{use}}} \begin{cases} > 1 - \dfrac{\eta_{\text{ORC-}n}}{\eta_{\text{ORC-}a}}, & \text{form (c) is better,} \\ = 1 - \dfrac{\eta_{\text{ORC-}n}}{\eta_{\text{ORC-}a}}, & \text{same,} \\ < 1 - \dfrac{\eta_{\text{ORC-}n}}{\eta_{\text{ORC-}a}}, & \text{form (d) is better.} \end{cases} \tag{25}$$

Therefore, the form of the cogeneration system is determined by the ratio between the heating load of buildings and the effective heat collection of the solar collector subsystem when the building heating load is less than the effective heat collection.

5. Results

5.1. Form of the Cogeneration System. According to the analysis in Section 4.2, no matter what type of the collector the cogeneration system adopts, the form is the same, as shown in Figure 10. V1~V5 are solenoid valves.

5.2. Operation Modes of the Cogeneration System. Although the form of the cogeneration system is the same for different types of the solar collectors, the operation modes are different for PTC and FPC or ETC.

5.2.1. When Solar Collectors Are PTC. There are six operating modes when the solar collectors are PTC based on the size relationship between the heating load of buildings and the effective heat collection of the solar collector subsystem, as shown in the following.

(1) PM1: for cloudy and rainy days, when the effective heat collection of the solar collector subsystem is 0. V1~V4 are off and V5 is on

(2) PM2: when the condensing heat of the ORC subsystem is less than the heating load and greater than 0. V1, V4, and V5 are on. V2 and V3 are off

(3) PM3: when the condensing heat of the ORC subsystem and the heating load are equal. V1 and V4 are on. V2, V3, and V5 are off

(4) PM4: when the condensing heat of the ORC subsystem is slightly greater than the heating load. V1, V3, and V4 are on. V2 and V5 are off

(5) PM5: when the condensing heat of the ORC subsystem is much greater than the heating load. V1, V2, and V3 are on. V4 and V5 are off

(6) PM6: for nonheating season, when the heating load is 0. V1 and V3 are on. V2, V4, and V5 are off

The specific state of the solenoid valves in different operating modes is shown in Table 4.

For example, when coefficients a_0, a_1, and a_2 of PTC are 0.762, 0.2125, and 0.001672, respectively, $t_{\text{col,in}}$ is 140°C, t_a is 15°C, $t_{n,h}$ is 40°C, and G_{eff} is 600 W/m^2, after the calculation, the value of $\eta_{\text{ORC-a}}$ is 0.1073, and the value of credited $\eta_{\text{ORC-n}}$ is 0.0844. That is, when the value of $Q_{\text{load}}/Q_{\text{use}}$ is greater than 0 and less than 0.213, the cogeneration system runs in PM5 mode. When the value of $Q_{\text{load}}/Q_{\text{use}}$ is equal to 0.213 or greater than 0.213 and less than 0.916, the cogeneration system runs in PM4 mode. When the value of $Q_{\text{load}}/Q_{\text{use}}$ is equal to 0.916, the cogeneration system runs in PM3 mode. When the value of $Q_{\text{load}}/Q_{\text{use}}$ is greater than 0.916, the system runs in PM2 mode, which is shown in Figure 11.

5.2.2. When Solar Collectors Are FPC or ETC. There are also six operating modes when the solar collectors are FPC or ETC based on the size relationship between the heating load of buildings and the effective heat collection of the solar collector subsystem, as shown in the following.

(1) TM1: for cloudy and rainy days, when the effective heat collection of the solar collector subsystem is 0. V1~V4 are off and V5 is on

(2) TM2: when the effective heat collection of the solar collector subsystem is less than the heating load and greater than 0. V2 and V5 are on. V1, V3, and V4 are off

(3) TM3: when the effective heat collection of the solar collector subsystem and the heating load are equal. V2 is on. V1, V3, V4, and V5 are off

(4) TM4: when the condensing heat of the ORC subsystem is slightly greater than the heating load. V1, V3, and V4 are on. V2 and V5 are off

(5) TM5: when the condensing heat of the ORC subsystem is much greater than the heating load. V1, V2, and V3 are on. V4 and V5 are off

(6) TM6: for nonheating season, when the heating load is 0. V1 and V3 are on. V2, V4, and V5 are off

The specific state of the solenoid valves in different operating modes is shown in Table 5. $Q_{\text{use}-n}$ is the heat collection when the inlet temperature of the solar

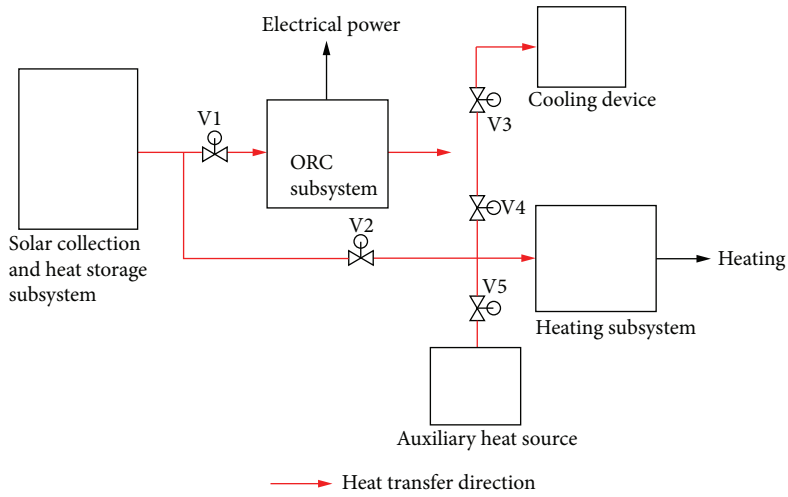

Figure 10: Form of the cogeneration system.

Table 4: The specific state of the solenoid valves in different operating modes when the solar collectors are PTC.

Operating modes	Operating conditions	V1	V2	V3	V4	V5
PM1	$Q_{use} = 0$	Off	Off	Off	Off	On
PM2	$Q_{load}/Q_{use} > 1 - \eta_{ORC\text{-}n}$	On	Off	Off	On	On
PM3	$Q_{load}/Q_{use} = 1 - \eta_{ORC\text{-}n}$	On	Off	Off	On	Off
PM4	$1 - \eta_{ORC\text{-}n} > Q_{load}/Q_{use} \geq 1 - \eta_{ORC\text{-}n}/\eta_{ORC\text{-}a}$	On	Off	On	On	Off
PM5	$Q_{load}/Q_{use} < 1 - \eta_{ORC\text{-}n}/\eta_{ORC\text{-}a}$	On	On	On	Off	Off
PM6	$Q_{load} = 0$	On	Off	On	Off	Off

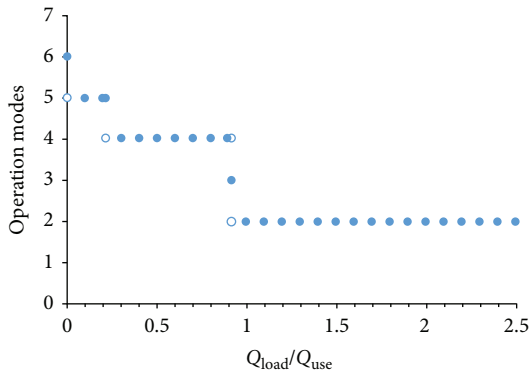

Figure 11: Operation modes of the cogeneration system at different Q_{load}/Q_{use}.

collectors is $t_{n,h}$. Q_{use-d} refers to the heat collection in the cogeneration mode, at which the operation temperature of the solar collectors is higher.

For example, when coefficients a_0 and a_1 of ETC are 0.82 and 2.19, respectively, $t_{col,in}$ is 110°C, t_a is 15°C, $t_{n,h}$ is 40°C, and G_{eff} is 600 W/m^2, after the calculation, the value of η_{ORC-a} is 0.0899, the value of η_{ORC-n} is 0.0669, the value of η_{col-n} is 0.7288, and the value of η_{col-d} is 0.4732. That is, when the value of Q_{load}/Q_{use-d} is greater than 0 and less than 0.255, the cogeneration system runs in TM5 mode. When the value of Q_{load}/Q_{use-d} is equal to 0.255 or greater than 0.255 and less than 0.933, the cogeneration system runs in TM4 mode. When the value of Q_{load}/Q_{use-d} is equal to 0.933 or greater than 0.933 and less than 1.54 or equal to 1.54, the cogeneration system runs in TM3 mode. When the value of Q_{load}/Q_{use-d} is greater than 1.54, the system runs in TM2 mode, which is shown in Figure 12.

6. Conclusions

This paper mainly analyzes the form and the operation mode of the solar-driven cogeneration system consisting of solar collectors (PTC, FPC, and ETC) and ORC based on the building heating load. The main results are as follows:

(1) A calculation model of the ORC power generation device is established, and the accuracy of the model is verified by the experimental data provided by an equipment manufacturer. Based on this calculation model, the fitting formula of the thermal efficiency of the ORC power generation device is obtained

(2) Both the optimal form and the optimal operation mode of the cogeneration system are determined.

Table 5: The specific state of the solenoid valves in different operating modes when the solar collectors are FPC or ETC.

Operating modes	Operating conditions	V1	V2	V3	V4	V5
TM1	$Q_{use\text{-}n} = 0$	Off	Off	Off	Off	On
TM2	$Q_{load} > Q_{use\text{-}n}$	Off	On	Off	Off	On
TM3	$Q_{use\text{-}n} \geq Q_{load} \geq Q_{use\text{-}d}(1 - \eta_{ORC\text{-}n})$	Off	On	Off	Off	Off
TM4	$1 - \eta_{ORC\text{-}n} > Q_{load}/Q_{use\text{-}d} \geq 1 - \eta_{ORC\text{-}n}/\eta_{ORC\text{-}a}$	On	Off	On	On	Off
TM5	$Q_{load}/Q_{use\text{-}d} < 1 - \eta_{ORC\text{-}n}/\eta_{ORC\text{-}a}$	On	On	On	Off	Off
TM6	$Q_{load} = 0$	On	Off	On	Off	Off

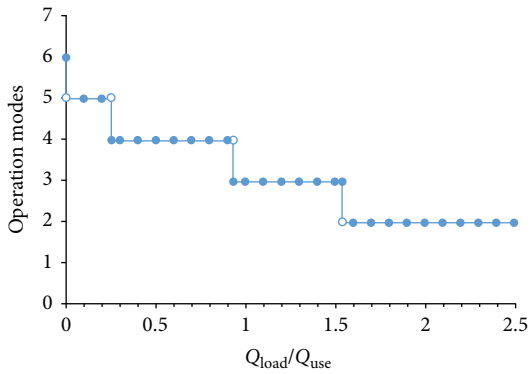

Figure 12: Operation modes of the cogeneration system at different Q_{load}/Q_{use-d}.

The optimal form is the same no matter which type of the collector (PTC, FPC, and ETC) the cogeneration system adopts, while the optimal operation modes are two kinds based on whether the coefficient a_1 of the solar collectors is less than 0.45, and only PTC meets the condition

(3) There are six operating modes when the solar collectors are PTC based on the ratio of the heating load of buildings (Q_{load}) and the effective heat collection of the solar collector subsystem (Q_{use}), namely, PM1~PM6 in this paper. When coefficients a_0, a_1, and a_2 of PTC are 0.762, 0.2125, and 0.001672, respectively, $t_{col,in}$ is 140°C, t_a is 15°C, $t_{n,h}$ is 40°C, and G_{eff} is 600 W/m^2, it can be obtained that the cogeneration system runs in PM5 mode if Q_{load}/Q_{use} is greater than 0 and less than 0.213; it runs in PM4 mode if Q_{load}/Q_{use} is equal to 0.213 or greater than 0.213 and less than 0.916; it runs in PM3 mode if Q_{load}/Q_{use} is 0.916, and it runs in PM2 mode if Q_{load}/Q_{use} is greater than 0.916

(4) There are also six operating modes when the solar collectors are FPC or ETC based on the ratio of the heating load of buildings (Q_{load}) and the effective heat collection of the solar collector subsystem (Q_{use-d}), namely, TM1~TM6 in this paper. When coefficients a_0 and a_1 of ETC are 0.82 and 2.19, respectively, $t_{col,in}$ is 110°C, t_a is 15°C, $t_{n,h}$ is 40°C, and G_{eff} is 600 W/m^2, it can be obtained that the cogeneration system runs in TM5 mode if Q_{load}/Q_{use-d} is greater than 0 and less than 0.255; it runs in TM4 mode if Q_{load}/Q_{use-d} is equal to 0.255 or greater than 0.255 and less than 0.933; it runs in TM3 mode if Q_{load}/Q_{use-d} is equal to 0.933 or greater than 0.933 and less than 1.54 or equal to 1.54, and it runs in TM2 mode if Q_{load}/Q_{use-d} is greater than 1.54

Nomenclature

A: Area (m^2)
c: Specific heat (kJ/kg·K)
G: Solar irradiance (W/m^2)
h: Enthalpy (kJ/kg)
m: Mass flow rate (kg/s)
Q: Heat rate (W)
t: Temperature (°C)
W: Power (kWh).

Greek Letters

η: Efficiency.

Subscripts and Superscripts

a:	Ambient
c:	Outlet water of air source heat pump
col:	Collector
cond:	Condenser
eff:	Effective
evap:	Evaporator
fa, fb, fc, fd:	Form (a), form (b), form (c), form (d)
g:	Supply water
h:	Return water
in:	Inlet
ise:	Isentropic
load:	Heating load of buildings
L:	Cooling source
mec:	Mechanical
n:	For heating
OP:	Organic pump
org:	Organic fluid
out:	Outlet
R:	Heating source
SE:	Screw expander
sol:	Solar energy
use:	Useful
wat:	Water.

Data Availability

The data used to support the findings of this study are included within the article.

Conflicts of Interest

The authors declare that there is no conflict of interest regarding the publication of this paper.

Acknowledgments

This study has been supported by the China National Key R&D Program "Key technologies and demonstration projects of building energy-saving in large-scale public transport buildings" (Grant no. 2018YFC0705001-6).

References

[1] L. Wang, L. Yuan, C. M. Zhu, Z. R. Li, and N. Y. Yu, "Necessity of the whole process commissioning for active solar heating systems," *Heating, Ventilating and Air Conditioning*, vol. 42, pp. 53–56, 2012.

[2] H. Zhai, Y. J. Dai, J. Y. Wu, and R. Z. Wang, "Energy and exergy analyses on a novel hybrid solar heating, cooling and power generation system for remote areas," *Applied Energy*, vol. 86, no. 9, pp. 1395–1404, 2009.

[3] F. A. Al-Sulaiman, I. Dincer, and F. Hamdullahpur, "Exergy modeling of a new solar driven trigeneration system," *Solar Energy*, vol. 85, no. 9, pp. 2228–2243, 2011.

[4] F. A. Al-Sulaiman, F. Hamdullahpur, and I. Dincer, "Performance assessment of a novel system using parabolic trough solar collectors for combined cooling, heating, and power production," *Renewable Energy*, vol. 48, pp. 161–172, 2012.

[5] F. A. Al-Sulaiman, "Exergy analysis of parabolic trough solar collectors integrated with combined steam and organic Rankine cycles," *Energy Conversion and Management*, vol. 77, pp. 441–449, 2014.

[6] H. D. Wang, "Performance evaluation of a small scale modular solar trigeneration system," *International Journal of Photoenergy*, vol. 2014, Article ID 964021, 9 pages, 2014.

[7] M. Al-Ali and I. Dincer, "Energetic and exergetic studies of a multigenerational solar–geothermal system," *Applied Thermal Engineering*, vol. 71, no. 1, pp. 16–23, 2014.

[8] S. A. Kalogirou, S. Karellas, K. Braimakis, C. Stanciu, and V. Badescu, "Exergy analysis of solar thermal collectors and processes," *Progress in Energy and Combustion Science*, vol. 56, pp. 106–137, 2016.

[9] S. A. Kalogirou, S. Karellas, V. Badescu, and K. Braimakis, "Exergy analysis on solar thermal systems: a better understanding of their sustainability," *Renewable Energy*, vol. 85, pp. 1328–1333, 2016.

[10] E. Bellos and C. Tzivanidis, "Parametric analysis and optimization of a solar driven trigeneration system based on ORC and absorption heat pump," *Journal of Cleaner Production*, vol. 161, pp. 493–509, 2017.

[11] J. Freeman, K. Hellgardt, and C. N. Markides, "Working fluid selection and electrical performance optimisation of a domestic solar-ORC combined heat and power system for year-round operation in the UK," *Applied Energy*, vol. 186, pp. 291–303, 2017.

[12] H. F. Zhang, B. Lei, T. Yu, and Z. D. Zhao, "Exergy analysis of two kinds of solar-driven cogeneration systems in Lhasa, Tibet, China," *International Journal of Photoenergy*, vol. 2018, Article ID 6702049, 11 pages, 2018.

[13] A. M. Delgado-Torres and L. García-Rodríguez, "Analysis and optimization of the low-temperature solar organic Rankine cycle (ORC)," *Energy Conversion and Management*, vol. 51, no. 12, pp. 2846–2856, 2010.

[14] X. D. Wang, L. Zhao, J. L. Wang, W. Z. Zhang, X. Z. Zhao, and W. Wu, "Performance evaluation of a low-temperature solar Rankine cycle system utilizing R245fa," *Solar Energy*, vol. 84, no. 3, pp. 353–364, 2010.

[15] X. D. Wang, L. Zhao, and J. L. Wang, "Experimental investigation on the low-temperature solar Rankine cycle system using R245fa," *Energy Conversion and Management*, vol. 52, no. 2, pp. 946–952, 2011.

[16] Y. L. He, D. H. Mei, W. Q. Tao, W. W. Yang, and H. L. Liu, "Simulation of the parabolic trough solar energy generation system with organic Rankine cycle," *Applied Energy*, vol. 97, pp. 630–641, 2012.

[17] G. Pei, J. Li, and J. Ji, "Analysis of low temperature solar thermal electric generation using regenerative organic Rankine cycle," *Applied Thermal Engineering*, vol. 30, no. 8-9, pp. 998–1004, 2010.

[18] G. Pei, J. Li, and J. Ji, "Design and analysis of a novel low-temperature solar thermal electric system with two-stage collectors and heat storage units," *Renewable Energy*, vol. 36, no. 9, pp. 2324–2333, 2011.

[19] G. Cau and D. Cocco, "Comparison of medium-size concentrating solar power plants based on parabolic trough and linear Fresnel collectors," *Energy Procedia*, vol. 45, pp. 101–110, 2014.

[20] F. Ruzzenenti, M. Bravi, D. Tempesti, E. Salvatici, G. Manfrida, and R. Basosi, "Evaluation of the environmental sustainability of a micro CHP system fueled by low-temperature geothermal and solar energy," *Energy Conversion and Management*, vol. 78, pp. 611–616, 2014.

[21] A. Baccioli, M. Antonelli, and U. Desideri, "Dynamic modeling of a solar ORC with compound parabolic collectors: annual production and comparison with steady-state simulation," *Energy Conversion and Management*, vol. 148, pp. 708–723, 2017.

[22] S. Kalogirou, "The potential of solar industrial process heat applications," *Applied Energy*, vol. 76, no. 4, pp. 337–361, 2003.

[23] S. Kalogirou, "Solar thermal collectors and applications," *Progress in Energy and Combustion Science*, vol. 30, no. 3, pp. 231–295, 2004.

[24] P. He and Y. J. Dai, "Optimization of high performance flat-plate solar collector," *Building Science*, vol. 31, pp. 58–61, 2015.

[25] S. F. Yan, C. Q. Yan, and H. K. Liu, "Study on thermal performance of typical solar collectors," *Solar Energy*, vol. 11, pp. 51–55, 2016.

[26] Y. Gao, X. X. Lin, and X. Y. Zhang, "System dynamic performance comparison of two types of all-glass evacuated tube solar collectors," *Acta Energiae Solaris Sinica*, vol. 37, pp. 1461–1467, 2016.

[27] Y. M. Zhuang, "The energy consumption and economical analysis for evaporative condenser compared to shell-tube water-cooling condensers," *Refrigeration*, vol. 20, pp. 48–51, 2001.